EUROPEAN ORGANIZATION FOR NUCLEAR RESEARCH

CERN-PPE/97-52
7 May 1997

Measurement of Hadron and Lepton–Pair Production at 161 GeV $< \sqrt{s} <$ 172 GeV at LEP

L3 Collaboration

Abstract

We report on measurements of e^+e^- annihilation into hadrons and lepton pairs. The data have been taken with the L3 detector at LEP at centre–of–mass energies between 161 GeV and 172 GeV. In a data sample corresponding to 21.2 pb^{-1} of integrated luminosity 2728 hadronic and 868 lepton–pair events are selected. The measured cross sections and leptonic forward–backward asymmetries agree well with the Standard Model predictions.

Submitted to *Phys. Lett. B*

1 Introduction

In 1996 LEP was operated for the first time at centre–of–mass energies above the W–pair production threshold. In July and August 10.9 pb^{-1} were collected at $\sqrt{s} = 161.3$ GeV. In October and November the centre–of–mass energy was increased and 1.0 pb^{-1} and 9.3 pb^{-1} were recorded at $\sqrt{s} = 170.3$ GeV and $\sqrt{s} = 172.3$ GeV, respectively. The small data sample taken at 170.3 GeV is combined with the data taken at 172.3 GeV for the measurements of muon and tau–pair production and the Bhabha asymmetry measurements.

In this article we report on measurements of the fermion pair production reactions:

$$\mathrm{e^+e^-} \to \mathrm{hadrons}(\gamma)\,, \quad \mathrm{e^+e^-} \to \mu^+\mu^-(\gamma)\,, \quad \mathrm{e^+e^-} \to \tau^+\tau^-(\gamma)\,, \quad \mathrm{e^+e^-} \to \mathrm{e^+e^-}(\gamma)\,. \quad (1)$$

In these reactions, the (γ) indicates the possible presence of additional photons. Cross sections are measured for all processes and forward–backward asymmetries for the lepton channels.

For a substantial fraction of the events initial–state radiation, ISR, photons are emitted. They lower the initial centre–of–mass energy to an effective centre–of–mass energy of the annihilation process, $\sqrt{s'}$. When $\sqrt{s'}$ is close to the Z mass, m_{Z}, the events are classed as radiative returns to the Z. A cut on $\sqrt{s'}$ allows a separation between events at high effective centre–of–mass energies, high energy events, and radiative returns to the Z.

For the total and the high energy event samples cross sections and asymmetries are measured and compared to the predictions of the Standard Model [1]. Combining the new results with our measurements at centre–of–mass energies around the Z–pole [2] and between 130 GeV and 140 GeV [3], the γZ interference and the Z–boson mass are determined with improved precision in the framework of the S–Matrix ansatz [4].

Similar studies have been presented for the data taken at 161 GeV by the OPAL collaboration [5].

2 Measurement of Fermion–Pair Production

The data were collected by the L3 detector described in [6]. The measurements of cross sections and forward–backward asymmetries are performed for the total and the high energy event samples. In the total event sample $\sqrt{s'}$ is required to be larger than $0.1\sqrt{s}$ to reduce uncertainties on radiative corrections in extrapolating to low $\sqrt{s'}$ values. The high energy sample is defined by requiring $\sqrt{s'} > 0.85\sqrt{s}$.

Using the sum of all ISR photon energies, E_γ, and momentum vectors, $\mathbf{P}_\gamma$, the $\sqrt{s'}$ value is given by:

$$s' \;=\; s - 2E_\gamma\sqrt{s} + E_\gamma^2 - \mathbf{P}_\gamma^2\,. \quad (2)$$

For most of the events the ISR photons are radiated along the beam pipe and are not detected. In this case the photon energy is determined assuming that a single photon is emitted along the beam axis. The $\sqrt{s'}$ value is estimated using Equation 2. The effect of multiple and final–state photon radiation on the $\sqrt{s'}$ calculation has been studied using Monte Carlo programs and is corrected for.

For the determination of selection efficiencies and backgrounds, Monte Carlo simulations are performed for each centre–of–mass energy using the following event generators: BHLUMI [7] (small angle Bhabha scattering); PYTHIA [8] ($\mathrm{e^+e^-} \to$ hadrons(γ), ZZ(γ), Zee(γ), We$\nu(\gamma)$); KORALZ [9] ($\mathrm{e^+e^-} \to \mu^+\mu^-(\gamma), \tau^+\tau^-(\gamma)$); BHAGENE [10] ($\mathrm{e^+e^-} \to \mathrm{e^+e^-}(\gamma)$); PHOJET [11]

(hadronic two–photon collisions); DIAG36 [12] ($e^+e^- \to e^+e^-\mu^+\mu^-$, $e^+e^-\tau^+\tau^-$, $e^+e^-e^+e^-$); KORALW [13] ($e^+e^- \to W^+W^-(\gamma)$), EXCALIBUR [14] ($e^+e^- \to q\bar{q}'e\nu(\gamma)$, $e^+e^- \to e^+e^-e^+e^-$); GGG [15] ($e^+e^- \to \gamma\gamma(\gamma)$).

The measurements are compared to the predictions of the Standard Model calculated using ZFITTER [16] and TOPAZ0 [17] with the following parameters: $m_Z = 91.195$ GeV [2], $\alpha_s(m_Z^2) = 0.123$ [18], $m_t = 175$ GeV [19], $\alpha(m_Z^2) = 1/128.896$ [20] and $m_H = 300$ GeV. The theoretical uncertainties of the Standard Model predictions are well below the one percent level [21] except for the predictions for the large angle Bhabha scattering which has an uncertainty of 2% [22].

The analyses of the different channels are similar to those performed at centre–of–mass energies between 130 GeV and 140 GeV [3]. Changes due to detector modifications and different background conditions at the increased centre–of–mass energies are discussed in the descriptions of the individual analyses.

2.1 Integrated Luminosity

The luminosity is measured using small–angle Bhabha scattering within a polar angular range of 35.0 mrad $< \theta <$ 61.8 mrad[1)]. The main systematic uncertainties originate from the event selection criteria, 0.4%, and from the limited knowledge of the detector geometry, 0.3%. Including the contribution from Monte Carlo statistics a total experimental uncertainty of 0.6% is assigned to the measurement of the integrated luminosity. The theoretical uncertainty of the BHLUMI generator is less than 0.25% for the centre–of–mass energies given above [7].

2.2 $e^+e^- \to$ hadrons(γ)

Event Selection

Events are selected by restricting the visible energy, E_{vis}, to $0.4 < E_{vis}/\sqrt{s} < 2.0$. The longitudinal energy imbalance must satisfy $|E_{long}|/E_{vis} < 0.7$. There must be more than 11 calorimetric clusters with an energy larger than 300 MeV. In order to reject noise and background from cosmic muons, an energy of at least 15 GeV must be deposited in the electromagnetic calorimeter and at least 4 tracks from the interaction point must be reconstructed in the central tracker.

At centre–of–mass energies of 170 GeV and 172 GeV background from W–pair production is reduced by applying the following cuts. Semi leptonic W–pair decays are rejected by requiring the transverse energy imbalance to be smaller than 0.3 E_{vis}. Events in the high energy sample with at least four jets each with energy larger than 15 GeV are rejected to decrease the background from hadronic W–pair decays. The jets are obtained using the JADE algorithm [23] with a fixed jet resolution parameter $y_{cut} = 0.01$.

In Figure 1 the most important selection variable is shown for the different final states. In Figure 1a the distribution of the visible energy normalised to the centre–of–mass energy for hadronic final state events selected at 172 GeV is shown. The double–peak structure of the signal arises from the high energy events and from the radiative returns to the Z. A good agreement between data and Monte Carlo expectation is found.

To calculate the effective centre–of–mass energy, all events are reclustered into two jets using the JADE algorithm. A kinematic fit is performed on the two jets and the missing energy vector

[1)] The analysis follows [2] with a tight fiducial volume on one side restricting the radial coordinate to 99.6 mm $< R <$ 176.2 mm and the azimuthal angle to $|90° - \phi| > 11.6°$, $|270° - \phi| > 11.6°$. The loose fiducial volume on the opposite side is given by: 92.0 mm $< R <$ 183.8 mm and $|90° - \phi| > 4°$, $|270° - \phi| > 4°$.

imposing four–momentum conservation. The direction of the missing energy vector is assumed to be parallel to the beam axis. The missing energy is attributed to a single ISR photon. For about 10% of the events, a photon is detected in the electromagnetic calorimeter. It must have an electromagnetic shower shape, an energy larger than 20 GeV and an angular separation of more than 10 degrees to the nearest energy cluster. The energy and momentum of this photon are added to those of the undetected ISR photon and the $\sqrt{s'}$ value is calculated according to Equation 2. In Figure 2 the reconstructed $\sqrt{s'}$ distribution is shown for the different final states. Figure 2a shows the $\sqrt{s'}$ distribution for hadronic final state events selected at 172 GeV.

Cross Section

Selection efficiencies and background contributions are listed in Table 1. After application of the selection criteria the sample contains a background from hadronic two–photon collision processes, W–, Z– and tau–pair production and $e^+e^- \to Zee(\gamma)$ events. The two–photon background is estimated by adjusting the Monte Carlo to the data in a background enriched sample.

Systematic errors of 1.1% for the total and 2.0% for the high energy event sample are assigned to the cross section measurements. They are dominated by the uncertainty on the two–photon background for the total data sample and by the uncertainty on the $\sqrt{s'}$ determination for the high energy sample. The uncertainty on the $\sqrt{s'}$ calculation is estimated by varying the $\sqrt{s'}$ cut.

The numbers of selected events and the total cross sections for the different event samples are listed in Table 2. In Figure 3 the cross section measurements are shown together with our previous measurements [2, 3] and are compared to the Standard Model predictions.

2.3 $e^+e^- \to \mu^+\mu^-(\gamma)$

Event Selection

The event selection for the process $e^+e^- \to \mu^+\mu^-(\gamma)$ follows that of [3] with minor modifications. The lower cut on the highest momentum measured in the muon chambers, $p_{\max}$, is set to a fixed value of 35 GeV to ensure high acceptance for events with hard ISR photons.

Background from cosmic muons is reduced by using scintillation counter time information. The number of accepted cosmic muon events is found to be 0.6 ± 0.2 at 161 GeV and 1.2 ± 0.3 at 172 GeV. In Figure 1b the distribution of the maximum muon momentum normalised to $E_{\rm beam}$ for events selected at 172 GeV is shown.

The $\sqrt{s'}$ value for each event is determined using Equation 2 assuming the emission of a single ISR photon. In case the photon is found in the detector it is required to have an energy, E_γ, larger than 10 GeV in the electromagnetic calorimeter and an angular separation to the nearest muon of more than 10 degrees. Otherwise the photon is assumed to be emitted along the beam axis and its energy is calculated from the polar angles, θ_1 and θ_2, of the outgoing muons:

$$E_\gamma \;=\; \sqrt{s} \cdot \frac{|\sin(\theta_1+\theta_2)|}{\sin\theta_1 + \sin\theta_2 + |\sin(\theta_1+\theta_2)|}\,, \tag{3}$$

The distribution of the reconstructed $\sqrt{s'}$ for events selected at 172 GeV is shown in Figure 2b. A good agreement between data and Monte Carlo expectation is found.

Cross Section

Selection efficiencies and background contributions are listed in Table 1. The main background contributions are from the reactions $e^+e^- \to e^+e^-\mu^+\mu^-, e^+e^- \to \tau^+\tau^-(\gamma)$ and from W–pair production. The background contributions include the contamination of the high energy event sample with events with hard ISR photons. The systematic error of the cross section measurement is estimated to be 4% for both the total and the high energy sample. The main contributions are the uncertainties on the background and acceptance corrections.

In Table 2 the number of selected events and the resulting cross sections for the two event samples at the different centre–of–mass energies are summarised. In Figure 4 the comparison to the Standard Model prediction is shown.

Forward–Backward Asymmetry

The forward–backward asymmetry is determined using events with two identified muons with opposite charge and an acollinearity angle smaller than 90 degrees. The angular distribution of the events is parametrised by

$$\frac{\mathrm{d}\sigma}{\mathrm{d}\cos\theta} \;\propto\; \frac{3}{8}(1+\cos^2\theta) + \overline{A}_{\mathrm{fb}}\cos\theta\,, \tag{4}$$

where θ is the polar angle of the outgoing fermion with respect to the incoming electron.

The asymmetry, $\overline{A}_{\mathrm{fb}}$, is determined from an unbinned maximum–likelihood fit of Equation 4 to the data within $|\cos\theta| \leq 0.9$. The muon charge is measured in the muon spectrometer. The effect of a wrong charge assignment is estimated for each event and taken into account in the fit procedure. The charge confusion per track, $2 \pm 1\%$, has a negligible effect on the asymmetry since only events with zero total charge are used.

For the total event sample the differential cross section is distorted by hard ISR photons. For the high energy sample the measured quantity, $\overline{A}_{\mathrm{fb}}$, directly gives the forward–backward asymmetry for the full solid angle, A_{fb}. To extract A_{fb} for the total event sample a correction, $c_{\mathrm{ex}} \equiv A_{\mathrm{fb}}/\overline{A}_{\mathrm{fb}} = 0.78 \pm 0.01$, obtained from Monte Carlo is applied.

The background from $e^+e^- \to \tau^+\tau^-(\gamma)$ is small and, assuming lepton universality, has no influence on the measurement because it has the same asymmetry as the signal. The other background contributions are taken into account and the correction is in all cases smaller than 0.07. For the high energy sample the correction includes the background from events with hard ISR photons as calculated from Monte Carlo. The systematic error on the forward–backward asymmetry is estimated to be 0.05. Its main contributions are the uncertainties on background and acceptance corrections.

Table 3 summarises the numbers of forward and backward events, the background corrections, and the corrected asymmetries. In Figure 4 the comparison of the corrected asymmetries to the Standard Model prediction is shown.

2.4 $e^+e^- \to \tau^+\tau^-(\gamma)$

Event Selection

Taus are identified as narrow, low multiplicity jets, containing at least one charged particle. Tau jets are formed by matching the energy depositions in the electromagnetic and hadron calorimeters with tracks in the central tracker and the muon spectrometer. Two tau jets of at least 3.5 GeV are required to lie within the polar angular range $|\cos\theta| < 0.92$.

The reconstruction of $\sqrt{s'}$ follows the procedure described in Section 2.3 using the polar angles of the two tau jets. Events with one–one, one–three and three–three prong topologies are accepted. To allow for reconstruction inefficiencies one tau jet may also have 2 tracks and one–four topology events are accepted. One–one topology events are rejected if at least one of the tau jets lies in the region $0.72 < |\cos\theta| < 0.80$, which is not completely covered by the electromagnetic calorimeter. Hadronic events are removed by requiring less than 13 calorimetric clusters. Bhabha events are rejected by requiring the two highest energy clusters in the electromagnetic calorimeter to have energies less than $0.4\sqrt{s'}$ and $0.25\sqrt{s'}$. Radiative Bhabha events and events from the process $e^+e^- \to e^+e^-e^+e^-$ are removed by rejecting events with two identified electrons. Electrons are identified as a cluster in the electromagnetic calorimeter with energy larger than 3 GeV, with electromagnetic shower shape, and a matched track in the central tracker. All events with more than one reconstructed track in the muon chambers are removed. The energy of a reconstructed muon has to be less than $0.45\sqrt{s'}$.

To reject background from two–photon collisions only events with a $\sqrt{s'}$ larger than 60 GeV are accepted. In addition the quadratic sum of the energies of the tau jets, $E_{\rm jets} = \sqrt{E^2_{\rm jet1} + E^2_{\rm jet2}}$, has to be larger than $0.15\sqrt{s'}$. In Figure 1c the $E_{\rm jets}/\sqrt{s'}$ distribution for events selected at 172 GeV is shown.

To reject leptonic final states from W–pair production the acoplanarity of the two tau jets must be less than 15 degrees. The background from cosmic muons is reduced by using scintillation counter time information. The total energy in the electromagnetic calorimeter has to exceed 4 GeV. Applying this selection the $\sqrt{s'}$ distribution as shown in Figure 2c for events selected at 172 GeV is obtained. Good agreement between data and Monte Carlo expectation is found.

Cross Section

Selection efficiencies and backgrounds are listed in Table 1. The total systematic error which is dominated by the uncertainty on the background from two–photon collision processes is estimated to be 7% for both the total and the high energy sample.

The number of selected events and the total cross sections for the different event samples are listed in Table 2. The cross section measurements are compared to the Standard Model prediction in Figure 4.

Forward–Backward Asymmetry

For the determination of the forward–backward asymmetry, events with zero charge sum and an acollinearity angle between the two tau jets of less than 90 degrees are used. The procedure to obtain the forward–backward asymmetry is described in Section 2.3. The corresponding correction, $c_{\rm ex}$, is 0.92 ± 0.01.

The charge confusion of the events is estimated from the data to be $2.1 \pm 0.2\%$ for the total and $2.5 \pm 0.3\%$ for the high energy sample, and is corrected for. The asymmetries are corrected for backgrounds and the correction is in all cases smaller than 0.07. For the high energy sample, the correction includes the effect of the contamination from events with hard ISR photons. The systematic error on the forward–backward asymmetry is estimated to be 0.10. Its contributions are the uncertainties from the background and acceptance corrections and from the charge confusion.

In Table 3 the number of forward and backward events and the corrected asymmetries are given. In Figure 4 the comparison of the corrected asymmetries to the Standard Model

predictions is shown.

2.5 $e^+e^- \to e^+e^-(\gamma)$

Event Selection

Electron candidates are recognised by an energy deposition in the electromagnetic calorimeter with at least five associated hits in the central tracking chamber within a three degree cone. In addition only electrons within the polar angular range $44^\circ < \theta < 136^\circ$ are accepted.

Bhabha events are selected by requiring the two highest energy electrons to have an energy larger than $0.6\,E_{\rm beam}$ and 5 GeV, respectively. The acollinearity of the two electrons must be smaller than 90 degrees. In Figure 1d the energy of the highest energy electron candidate, $E_{\rm electron}$, normalised to the beam energy for events selected at 172 GeV is shown.

The $\sqrt{s'}$ value is reconstructed from the invariant mass of the two identified electrons. Its distribution is shown in Figure 2d for events selected at 172 GeV. The largest part of the events is from the t–channel exchange for which the $\sqrt{s'}$ value is close to the centre–of–mass energy.

Cross Section

The selection efficiencies within the fiducial volume and the background contributions are listed in Table 1. The background is from tau–pair production. The total systematic error of 3% assigned to the cross section measurements is dominated by uncertainties in the event selection.

In Table 2 the number of selected events and the resulting cross sections for the two event samples at the different centre–of–mass energies are summarised. The cross sections are compared to the Standard Model prediction in Figure 5.

Forward–Backward Asymmetry

The electron direction in the event is determined using a combined fit to both tracks as described in [2]. The average charge confusion of the events is measured from the data to be $(5.0 \pm 0.5)\%$ and is corrected for.

The forward–backward asymmetry is measured by counting events in the forward and backward hemispheres. In Table 3 the numbers of forward and backward events and the corrected asymmetries are summarised. The systematic error on the measured asymmetry is estimated to be 0.012 and is dominated by the uncertainty on the charge confusion. In Figure 5 the comparison of the measured asymmetries to the Standard Model prediction is shown.

The differential cross sections for the high energy samples at the different centre–of–mass energies are shown in Figure 6. A binned maximum–likelihood fit to the $\cos\theta$ distributions is performed to determine the s–channel asymmetry for the high energy event sample in the full solid angle. The dominant t–channel and s/t interference contributions are fixed to their Standard Model expectations. The resulting asymmetries are $0.3^{+\,0.4}_{-\,0.5}$ and $0.6^{+\,0.4}_{-\,0.6}$ for the data taken at centre–of–mass energies of 161 GeV and 172 GeV, respectively. These values agree with the Standard Model expectation which is 0.6 at both centre–of–mass energies.

3 Determination of the γZ Interference

The data is interpreted in the framework of the S–Matrix ansatz [4], which makes a minimum of theoretical assumptions. The programs SMATASY [24] together with ZFITTER and TOPAZ0,

are used for the calculation of the theoretical predictions and QED radiative corrections of cross sections and forward–backward asymmetries.

The lowest–order total cross section, $\sigma^0_{\rm tot}$, and forward–backward asymmetry, $A^0_{\rm fb}$, for $\rm e^+e^- \to f\overline{f}$ [4] are:

$$\begin{aligned} \sigma^0_a(s) &= \frac{4}{3}\pi\alpha^2 \left[\frac{\rm g^a_f}{s} + \frac{\rm j^a_f (s-\overline{m}^2_Z) + r^a_f\, s}{(s-\overline{m}^2_Z)^2 + \overline{m}^2_Z \overline{\Gamma}^2_Z} \right] \qquad \text{for } a = \text{tot, fb} \\ A^0_{\rm fb}(s) &= \frac{3}{4}\frac{\sigma^0_{\rm fb}(s)}{\sigma^0_{\rm tot}(s)}\,. \end{aligned}$$

The S–Matrix ansatz defines the Z resonance using a Breit–Wigner denominator with s–independent width. In other approaches usually a Breit–Wigner denominator with s–dependent width is used which implies the following transformation of the values of the Z boson mass and width [4]: $m_Z = \overline{m}_Z + 34.1$ MeV and $\Gamma_Z = \overline{\Gamma}_Z + 0.9$ MeV. In the following the fit results are quoted after applying these transformations. The S–Matrix parameters $\rm r_f$, $\rm j_f$ and $\rm g_f$ scale the Z exchange, γZ interference and γ exchange contributions. Here the γ exchange contributions $\rm g_f$ are fixed to their QED predictions.

The S–Matrix parameters are determined in a χ^2 fit to the measurements presented here and to our previously published measurements [2, 3]. The uncertainties on the LEP beam energy of 27 MeV and 30 MeV for the 161 GeV and 172 GeV data [25], respectively, have a negligible effect on the fit results.

The fitted S–Matrix parameters for electrons, muons, taus and hadrons, and their correlations, are listed in Tables 4 and 5. The fits are performed with and without the assumption of lepton universality. The parameters obtained for the individual leptons are compatible with each other and support this assumption.

A large correlation, -43%, is found between the mass of the Z boson and the hadronic γZ interference term, $\rm j^{tot}_{had}$. This correlation causes an increase in the error on m_Z with respect to fits where the hadronic γZ interference term is fixed to its Standard Model prediction [2, 26, 27]. Under the assumption of lepton universality the fitted hadronic γZ interference term is:

$$\rm j^{tot}_{had} = 0.39 \pm 0.29\,,$$

which agrees with the Standard Model prediction of 0.22 and improves the precision of our previous result [3] significantly. The fitted value for m_Z is:

$$m_Z = 91193 \pm 9 \pm 3 \ \text{MeV}\,.$$

The contribution of the uncertainty on the γZ interference has been separated from the total experimental error and is quoted as the second error. It is reduced by a factor of 2 with respect to our previous publication [3]. Figure 7 shows the 68% confidence level contours in the (m_Z, $\rm j^{tot}_{had}$) plane for the data taken at the Z–pole and after including the 130–172 GeV measurements. The improvement arising from the high energy measurements is clearly visible.

4 Summary and Conclusion

Based on an integrated luminosity of 21.2 $\rm pb^{-1}$ collected at centre–of–mass energies between 161 GeV and 172 GeV, we select 2728 hadronic and 868 lepton–pair events. The data is used to measure cross sections and leptonic forward–backward asymmetries. The measurements are performed for the total event sample and for the high energy sample. The results are in good agreement with the Standard Model. Our measurements provide an improved determination of the γZ interference terms and the Z–boson mass within the S–Matrix framework.

Acknowledgements

We wish to congratulate the CERN accelerator divisions for the successful upgrade of the LEP machine and to express our gratitude for the excellent performance of the machine. We acknowledge the effort of all engineers, technicians and support staff who have participated in the construction and maintenance of this experiment. Those of us who are not from member states thank CERN for its hospitality and help.

References

[1] S.L. Glashow Nucl. Phys. **22** (1961) 579;
S. Weinberg, Phys. Rev. Lett. **19** (1967) 1264;
A. Salam, *Elementary Particle Theory*, ed. N. Svartholm, Stockholm, Almquist & Wiksell (1968) 367.

[2] L3 Collab., M. Acciarri *et al.*, Z. Phys. **C 62** (1994) 551.

[3] L3 Collab., M. Acciarri *et al.*, Phys. Lett. **B 370** (1996) 195.

[4] A. Leike, T. Riemann and J. Rose, Phys. Lett. **B 273** (1991) 513;
T. Riemann, Phys. Lett. **B 293** (1992) 451.

[5] OPAL Collab., K. Ackerstaff *et al.*, *Production of Fermion–pair Events in e^+ e^- Collision at 161 GeV Centre–of–mass Energy*, Preprint CERN-PPE/96–156, submitted to Phys. Lett. B.

[6] L3 Collab., B. Adeva *et al.*, Nucl. Inst. Meth. **A 289** (1990) 35;
M. Acciarri *et al.*, Nucl. Inst. Meth. **A 351** (1994) 300;
M. Chemarin *et al.*, Nucl. Inst. Meth. **A 349** (1994) 345;
A. Adam *et al.*, Preprint CERN-PPE/96–097 to be published in Nucl. Inst. Meth;
I.C. Brock *et al.*, Nucl. Inst. Meth. **A 381** (1996) 236.

[7] BHLUMI version 4.04 is used.
S. Jadach *et al.*, Comp. Phys. Comm. **70** (1992) 305; Phys. Lett. **B 353** (1995) 349; Phys. Lett. **B 353** (1995) 362; Preprint CERN-TH/96-158, submitted to Comp. Phys. Comm.

[8] T. Sjöstrand, *PYTHIA 5.7 and JETSET 7.4 Physics and Manual*, CERN–TH/7112/93 (1993), revised August 1995; Comp. Phys. Comm. **82** (1994) 74.

[9] KORALZ version 4.01 is used.
S. Jadach, B.F.L. Ward and Z. Wąs, Comp. Phys. Comm. **79** (1994) 503.

[10] BHAGENE version 3 is used.
J.H. Field, Phys. Lett. **B 323** (1994) 432;
J.H. Field and T. Riemann, Comp. Phys. Comm. **94** (1996) 53.

[11] PHOJET version 1.05 is used.
R. Engel, Z. Phys. **C 66** (1995) 203;
R. Engel and J. Ranft, Phys. Rev. **D 54** (1996) 4244.

[12] F.A. Berends, P.H. Daverfeldt and R. Kleiss, Nucl. Phys. **B 253** (1985) 441.

[13] KORALW version 1.21 is used.
M. Skrzypek, S. Jadach, W. Placzek and Z. Wąs, Comp. Phys. Comm. **94** (1996) 216;
M. Skrzypek, S. Jadach, M. Martinez, W. Placzek and Z. Wąs, Phys. Lett. **B 372** (1996) 289.

[14] F.A. Berends, R. Kleiss and R. Pittau, Nucl. Phys. **B 424** (1994) 308; Nucl. Phys. **B 426** (1994) 344; Nucl. Phys. (Proc. Suppl.) **B 37** (1994) 163; Phys. Lett. **B 335** (1994) 490; Comp. Phys. Comm. **83** (1994) 141.

[15] F.A. Berends and R. Kleiss, Nucl. Phys. **B 186** (1981) 22.

[16] ZFITTER version 5.0 is used.
D. Bardin *et al.*, Preprint CERN–TH/6443/92; Z. Phys. **C 44** (1989) 493; Nucl. Phys. **B 351** (1991) 1; Phys. Lett. **B 255** (1991) 290.

[17] TOPAZ0 version 2.0 is used.
G. Montagna, O. Nicrosini, G. Passarino, F. Piccinini and R. Pittau, Nucl. Phys. **B401** (1993) 3; Comp. Phys. Comm. **76** (1993) 328.

[18] L3 Collab., O. Adriani *et al.*, Physics Reports **236** (1993) 1.

[19] CDF Collab., 'Measurement of the Top Quark Mass at CDF', contributed paper to ICHEP96, PA-08-018;
DØ Collab., 'Measurement of the Top Mass from Events with Two Isolated Leptons Produced in $p\bar{p}$ Collisions at DØ', contributed paper to ICHEP96, PA-05-027;
DØ Collab., 'Measurement of the Top Mass from Events with Single Isolated Leptons Produced in $p\bar{p}$ Collisions at DØ', contributed paper to ICHEP96, PA-05-028.
P. Grannis, talk presented at ICHEP96, to appear in the proceedings.

[20] S. Eidelman and F. Jegerlehner, Z. Phys. **C 67** (1995) 585.

[21] E. Accomando *et al.*, in Physics at LEP2, Vol. 1, ed. T. Sjöstrand G. Altarelli and F. Zwirner, (Yellow Report: CERN 96-01, 1996), p. 207.

[22] H. Anlauf *et al.*, in Physics at LEP2, Vol. 2, ed. T. Sjöstrand G. Altarelli and F. Zwirner, (Yellow Report: CERN 96-01, 1996), p. 229.

[23] JADE Collab., W. Bartel *et al.*, Z. Phys. **C 33** (1986) 23;
JADE Collab., S. Bethke *et al.*, Phys. Lett. **B 213** (1988) 235.

[24] SMATASY version 5.0 is used.
S. Kirsch and T. Riemann, Comp. Phys. Comm. **88** (1995) 89.

[25] The Working Group on LEP Energy, private communication.

[26] L3 Collab., O. Adriani *et al.*, Phys. Lett. **B 315** (1993) 494.

[27] G. Isidori, Phys. Lett. **B 314** (1993) 139;
M. Grünewald and S. Kirsch, Preprint CERN–PPE/93–188 (1993).

The L3 Collaboration:

M.Acciarri,[29] O.Adriani,[18] M.Aguilar-Benitez,[28] S.Ahlen,[12] J.Alcaraz,[28] G.Alemanni,[24] J.Allaby,[19] A.Aloisio,[31] G.Alverson,[13] M.G.Alviggi,[31] G.Ambrosi,[21] H.Anderhub,[51] V.P.Andreev,[7,40] T.Angelescu,[14] F.Anselmo,[10] A.Arefiev,[30] T.Azemoon,[3] T.Aziz,[11] P.Bagnaia,[39] L.Baksay,[46] S.Banerjee,[11] Sw.Banerjee,[11] K.Banicz,[48] A.Barczyk,[51,49] R.Barillère,[19] L.Barone,[39] P.Bartalini,[36] A.Baschirotto,[29] M.Basile,[10] R.Battiston,[36] A.Bay,[24] F.Becattini,[18] U.Becker,[17] F.Behner,[51] J.Berdugo,[28] P.Berges,[17] B.Bertucci,[36] B.L.Betev,[51] S.Bhattacharya,[11] M.Biasini,[19] A.Biland,[51] G.M.Bilei,[36] J.J.Blaising,[4] S.C.Blyth,[37] G.J.Bobbink,[2] R.Bock,[1] A.Böhm,[1] L.Boldizsar,[15] B.Borgia,[39] D.Bourilkov,[51] M.Bourquin,[21] S.Braccini,[21] J.G.Branson,[42] V.Brigljevic,[51] I.C.Brock,[37] A.Buffini,[18] A.Buijs,[47] J.D.Burger,[17] W.J.Burger,[21] J.Busenitz,[46] A.Button,[3] X.D.Cai,[17] M.Campanelli,[51] M.Capell,[17] G.Cara Romeo,[10] G.Carlino,[31] A.M.Cartacci,[18] J.Casaus,[28] G.Castellini,[18] F.Cavallari,[39] N.Cavallo,[31] C.Cecchi,[21] M.Cerrada,[28] F.Cesaroni,[25] M.Chamizo,[28] Y.H.Chang,[53] U.K.Chaturvedi,[20] S.V.Chekanov,[33] M.Chemarin,[27] A.Chen,[53] G.Chen,[8] G.M.Chen,[8] H.F.Chen,[22] H.S.Chen,[8] X.Chereau,[4] G.Chiefari,[31] C.Y.Chien,[5] L.Cifarelli,[41] F.Cindolo,[10] C.Civinini,[18] I.Clare,[17] R.Clare,[17] H.O.Cohn,[34] G.Coignet,[4] A.P.Colijn,[2] N.Colino,[28] V.Commichau,[1] S.Costantini,[9] F.Cotorobai,[14] B.de la Cruz,[28] A.Csilling,[15] T.S.Dai,[17] R.D'Alessandro,[18] R.de Asmundis,[31] A.Degré,[4] K.Deiters,[49] D.della Volpe,[31] P.Denes,[38] F.DeNotaristefani,[39] D.DiBitonto,[46] M.Diemoz,[39] D.van Dierendonck,[2] F.Di Lodovico,[51] C.Dionisi,[39] M.Dittmar,[51] A.Dominguez,[42] A.Doria,[31] M.T.Dova,[20,♯] D.Duchesneau,[4] P.Duinker,[2] I.Duran,[43] S.Dutta,[11] S.Easo,[36] Yu.Efremenko,[34] H.El Mamouni,[27] A.Engler,[37] F.J.Eppling,[17] F.C.Erné,[2] J.P.Ernenwein,[27] P.Extermann,[21] M.Fabre,[49] R.Faccini,[39] S.Falciano,[39] A.Favara,[18] J.Fay,[27] O.Fedin,[40] M.Felcini,[51] B.Fenyi,[46] T.Ferguson,[37] F.Ferroni,[39] H.Fesefeldt,[1] E.Fiandrini,[36] J.H.Field,[21] F.Filthaut,[37] P.H.Fisher,[17] I.Fisk,[42] G.Forconi,[17] L.Fredj,[21] K.Freudenreich,[51] C.Furetta,[29] Yu.Galaktionov,[30,17] S.N.Ganguli,[11] P.Garcia-Abia,[50] S.S.Gau,[13] S.Gentile,[39] N.Gheordanescu,[14] S.Giagu,[39] S.Goldfarb,[24] J.Goldstein,[12] Z.F.Gong,[22] A.Gougas,[5] G.Gratta,[35] M.W.Gruenewald,[9] V.K.Gupta,[38] A.Gurtu,[11] L.J.Gutay,[48] B.Hartmann,[1] A.Hasan,[32] D.Hatzifotiadou,[10] T.Hebbeker,[9] A.Hervé,[19] W.C.van Hoek,[33] H.Hofer,[51] S.J.Hong,[45] H.Hoorani,[37] S.R.Hou,[53] G.Hu,[5] V.Innocente,[19] K.Jenkes,[1] B.N.Jin,[8] L.W.Jones,[3] P.de Jong,[19] I.Josa-Mutuberria,[28] A.Kasser,[24] R.A.Khan,[20] D.Kamrad,[50] Yu.Kamyshkov,[34] J.S.Kapustinsky,[26] Y.Karyotakis,[4] M.Kaur,[20,◇] M.N.Kienzle-Focacci,[21] D.Kim,[39] D.H.Kim,[45] J.K.Kim,[45] S.C.Kim,[45] Y.G.Kim,[45] W.W.Kinnison,[26] A.Kirkby,[35] D.Kirkby,[35] J.Kirkby,[19] D.Kiss,[15] W.Kittel,[33] A.Klimentov,[17,30] A.C.König,[33] A.Kopp,[50] I.Korolko,[30] V.Koutsenko,[17,30] R.W.Kraemer,[37] W.Krenz,[1] A.Kunin,[17,30] P.Ladron de Guevara,[28] I.Laktineh,[27] G.Landi,[18] C.Lapoint,[17] K.Lassila-Perini,[51] P.Laurikainen,[23] M.Lebeau,[19] A.Lebedev,[17] P.Lebrun,[27] P.Lecomte,[51] P.Lecoq,[19] P.Le Coultre,[51] J.M.Le Goff,[19] R.Leiste,[50] E.Leonardi,[39] P.Levtchenko,[40] C.Li,[22] C.H.Lin,[53] W.T.Lin,[53] F.L.Linde,[2,19] L.Lista,[31] Z.A.Liu,[8] W.Lohmann,[50] E.Longo,[39] W.Lu,[35] Y.S.Lu,[8] K.Lübelsmeyer,[1] C.Luci,[39] D.Luckey,[17] L.Luminari,[39] W.Lustermann,[49] W.G.Ma,[22] M.Maity,[11] G.Majumder,[11] L.Malgeri,[39] A.Malinin,[30] C.Maña,[28] D.Mangeol,[33] S.Mangla,[11] P.Marchesini,[51] A.Marin,[12] J.P.Martin,[27] F.Marzano,[39] G.G.G.Massaro,[2] D.McNally,[19] R.R.McNeil,[7] S.Mele,[31] L.Merola,[31] M.Meschini,[18] W.J.Metzger,[33] M.von der Mey,[1] Y.Mi,[24] A.Mihul,[14] A.J.W.van Mil,[33] G.Mirabelli,[39] J.Mnich,[19] P.Molnar,[9] B.Monteleoni,[18] R.Moore,[3] S.Morganti,[39] T.Moulik,[11] R.Mount,[35] S.Müller,[1] F.Muheim,[21] A.J.M.Muijs,[2] S.Nahn,[17] M.Napolitano,[31] F.Nessi-Tedaldi,[51] H.Newman,[35] T.Niessen,[1] A.Nippe,[1] A.Nisati,[39] H.Nowak,[50] Y.D.Oh,[45] H.Opitz,[1] G.Organtini,[39] R.Ostonen,[23] C.Palomares,[28] D.Pandoulas,[1] S.Paoletti,[39] P.Paolucci,[31] H.K.Park,[37] I.H.Park,[45] G.Pascale,[39] G.Passaleva,[18] S.Patricelli,[31] T.Paul,[13] M.Pauluzzi,[36] C.Paus,[1] F.Pauss,[51] D.Peach,[19] Y.J.Pei,[1] S.Pensotti,[29] D.Perret-Gallix,[4] B.Petersen,[33] S.Petrak,[9] A.Pevsner,[5] D.Piccolo,[31] M.Pieri,[18] J.C.Pinto,[37] P.A.Piroué,[38] E.Pistolesi,[29] V.Plyaskin,[30] M.Pohl,[51] V.Pojidaev,[30,18] H.Postema,[17] N.Produit,[21] D.Prokofiev,[40] G.Rahal-Callot,[51] N.Raja,[11] P.G.Rancoita,[29] M.Rattaggi,[29] G.Raven,[42] P.Razis,[32] K.Read,[34] D.Ren,[51] M.Rescigno,[39] S.Reucroft,[13] T.van Rhee,[47] S.Riemann,[50] K.Riles,[3] A.Robohm,[51] J.Rodin,[17] B.P.Roe,[3] L.Romero,[28] S.Rosier-Lees,[4] Ph.Rosselet,[24] W.van Rossum,[47] S.Roth,[1] J.A.Rubio,[19] D.Ruschmeier,[9] H.Rykaczewski,[51] J.Salicio,[19] E.Sanchez,[28] M.P.Sanders,[33] M.E.Sarakinos,[23] S.Sarkar,[11] M.Sassowsky,[1] C.Schäfer,[1] V.Schegelsky,[40] S.Schmidt-Kaerst,[1] D.Schmitz,[1] P.Schmitz,[1] N.Scholz,[51] H.Schopper,[52] D.J.Schotanus,[33] K.Schultze,[1] J.Schwenke,[1] G.Schwering,[1] C.Sciacca,[31] D.Sciarrino,[21] L.Servoli,[36] S.Shevchenko,[35] N.Shivarov,[44] V.Shoutko,[30] J.Shukla,[26] E.Shumilov,[30] A.Shvorob,[35] T.Siedenburg,[1] D.Son,[45] A.Sopczak,[50] B.Smith,[17] P.Spillantini,[18] M.Steuer,[17] D.P.Stickland,[38] A.Stone,[7] H.Stone,[38] B.Stoyanov,[44] A.Straessner,[1] K.Strauch,[16] K.Sudhakar,[11] G.Sultanov,[20] L.Z.Sun,[22] G.F.Susinno,[21] H.Suter,[51] J.D.Swain,[20] X.W.Tang,[8] L.Tauscher,[6] L.Taylor,[13] Samuel C.C.Ting,[17] S.M.Ting,[17] M.Tonutti,[1] S.C.Tonwar,[11] J.Tóth,[15] C.Tully,[38] H.Tuchscherer,[46] K.L.Tung,[8] Y.Uchida,[17] J.Ulbricht,[51] U.Uwer,[19] E.Valente,[39] R.T.Van de Walle,[33] G.Vesztergombi,[15] I.Vetlitsky,[30] G.Viertel,[51] M.Vivargent,[4] R.Völkert,[50] H.Vogel,[37] H.Vogt,[50] I.Vorobiev,[30] A.A.Vorobyov,[40] A.Vorvolakos,[32] M.Wadhwa,[6] W.Wallraff,[1] J.C.Wang,[17] X.L.Wang,[22] Z.M.Wang,[22] A.Weber,[1] F.Wittgenstein,[19] S.X.Wu,[20] S.Wynhoff,[1] J.Xu,[12] Z.Z.Xu,[22] B.Z.Yang,[22] C.G.Yang,[8] X.Y.Yao,[8] J.B.Ye,[22] S.C.Yeh,[53] J.M.You,[37] An.Zalite,[40] Yu.Zalite,[40] P.Zemp,[51] Y.Zeng,[1] Z.Zhang,[8] Z.P.Zhang,[22] B.Zhou,[12] G.Y.Zhu,[8] R.Y.Zhu,[35] A.Zichichi,[10,19,20] F.Ziegler.[50]

1 I. Physikalisches Institut, RWTH, D-52056 Aachen, FRG§
III. Physikalisches Institut, RWTH, D-52056 Aachen, FRG§
2 National Institute for High Energy Physics, NIKHEF, and University of Amsterdam, NL-1009 DB Amsterdam, The Netherlands
3 University of Michigan, Ann Arbor, MI 48109, USA
4 Laboratoire d'Annecy-le-Vieux de Physique des Particules, LAPP,IN2P3-CNRS, BP 110, F-74941 Annecy-le-Vieux CEDEX, France
5 Johns Hopkins University, Baltimore, MD 21218, USA
6 Institute of Physics, University of Basel, CH-4056 Basel, Switzerland
7 Louisiana State University, Baton Rouge, LA 70803, USA
8 Institute of High Energy Physics, IHEP, 100039 Beijing, China△
9 Humboldt University, D-10099 Berlin, FRG§
10 University of Bologna and INFN-Sezione di Bologna, I-40126 Bologna, Italy
11 Tata Institute of Fundamental Research, Bombay 400 005, India
12 Boston University, Boston, MA 02215, USA
13 Northeastern University, Boston, MA 02115, USA
14 Institute of Atomic Physics and University of Bucharest, R-76900 Bucharest, Romania
15 Central Research Institute for Physics of the Hungarian Academy of Sciences, H-1525 Budapest 114, Hungary‡
16 Harvard University, Cambridge, MA 02139, USA
17 Massachusetts Institute of Technology, Cambridge, MA 02139, USA
18 INFN Sezione di Firenze and University of Florence, I-50125 Florence, Italy
19 European Laboratory for Particle Physics, CERN, CH-1211 Geneva 23, Switzerland
20 World Laboratory, FBLJA Project, CH-1211 Geneva 23, Switzerland
21 University of Geneva, CH-1211 Geneva 4, Switzerland
22 Chinese University of Science and Technology, USTC, Hefei, Anhui 230 029, China△
23 SEFT, Research Institute for High Energy Physics, P.O. Box 9, SF-00014 Helsinki, Finland
24 University of Lausanne, CH-1015 Lausanne, Switzerland
25 INFN-Sezione di Lecce and Universitá Degli Studi di Lecce, I-73100 Lecce, Italy
26 Los Alamos National Laboratory, Los Alamos, NM 87544, USA
27 Institut de Physique Nucléaire de Lyon, IN2P3-CNRS,Université Claude Bernard, F-69622 Villeurbanne, France
28 Centro de Investigaciones Energeticas, Medioambientales y Tecnologicas, CIEMAT, E-28040 Madrid, Spain♭
29 INFN-Sezione di Milano, I-20133 Milan, Italy
30 Institute of Theoretical and Experimental Physics, ITEP, Moscow, Russia
31 INFN-Sezione di Napoli and University of Naples, I-80125 Naples, Italy
32 Department of Natural Sciences, University of Cyprus, Nicosia, Cyprus
33 University of Nijmegen and NIKHEF, NL-6525 ED Nijmegen, The Netherlands
34 Oak Ridge National Laboratory, Oak Ridge, TN 37831, USA
35 California Institute of Technology, Pasadena, CA 91125, USA
36 INFN-Sezione di Perugia and Universitá Degli Studi di Perugia, I-06100 Perugia, Italy
37 Carnegie Mellon University, Pittsburgh, PA 15213, USA
38 Princeton University, Princeton, NJ 08544, USA
39 INFN-Sezione di Roma and University of Rome, "La Sapienza", I-00185 Rome, Italy
40 Nuclear Physics Institute, St. Petersburg, Russia
41 University and INFN, Salerno, I-84100 Salerno, Italy
42 University of California, San Diego, CA 92093, USA
43 Dept. de Fisica de Particulas Elementales, Univ. de Santiago, E-15706 Santiago de Compostela, Spain
44 Bulgarian Academy of Sciences, Central Lab. of Mechatronics and Instrumentation, BU-1113 Sofia, Bulgaria
45 Center for High Energy Physics, Korea Adv. Inst. of Sciences and Technology, 305-701 Taejon, Republic of Korea
46 University of Alabama, Tuscaloosa, AL 35486, USA
47 Utrecht University and NIKHEF, NL-3584 CB Utrecht, The Netherlands
48 Purdue University, West Lafayette, IN 47907, USA
49 Paul Scherrer Institut, PSI, CH-5232 Villigen, Switzerland
50 DESY-Institut für Hochenergiephysik, D-15738 Zeuthen, FRG
51 Eidgenössische Technische Hochschule, ETH Zürich, CH-8093 Zürich, Switzerland
52 University of Hamburg, D-22761 Hamburg, FRG
53 High Energy Physics Group, Taiwan, China

§ Supported by the German Bundesministerium für Bildung, Wissenschaft, Forschung und Technologie
‡ Supported by the Hungarian OTKA fund under contract numbers T14459 and T24011.
♭ Supported also by the Comisión Interministerial de Ciencia y Tecnología
♯ Also supported by CONICET and Universidad Nacional de La Plata, CC 67, 1900 La Plata, Argentina
♢ Also supported by Panjab University, Chandigarh-160014, India
△ Supported by the National Natural Science Foundation of China.

	total [%]		high energy [%]	
	161 GeV	172 GeV	161 GeV	172 GeV
$\mathbf{e^+e^- \to hadrons(\gamma)}$				
Selection Efficiency	93.6	90.6	93.3	85.5
Two Photon Background	2.5	2.2	0.4	0.6
W^+W^- Background	1.9	6.7	4.2	5.0
Other Background	0.9	1.0	0.7	0.6
ISR Contamination	—	—	13.0	10.9
$\mathbf{e^+e^- \to \mu^+\mu^-(\gamma)}$				
Selection Efficiency	60.0	58.9	71.2	74.1
Two Photon Background	5.5	6.0	3.0	2.9
Cosmic Background	0.7	1.8	0.5	1.8
Other Background	1.8	4.0	2.6	3.8
ISR Contamination	—	—	7.7	6.5
$\mathbf{e^+e^- \to \tau^+\tau^-(\gamma)}$				
Selection Efficiency	31.9	30.8	44.8	44.1
Two Photon Background	12.8	13.0	5.4	7.4
Other Background	9.9	8.2	10.2	9.3
ISR Contamination	—	—	4.1	3.9
$\mathbf{e^+e^- \to e^+e^-(\gamma)}$				
Selection Efficiency	96.6	94.0	92.8	90.2
Background	0.5	1.0	< 0.1	< 0.1
ISR Contamination	—	—	0.4	0.4

Table 1: Selection efficiencies and background fractions for the total, $\sqrt{s'} > 0.1\sqrt{s}$, and the high energy, $\sqrt{s'} > 0.85\sqrt{s}$, event samples of the reactions $e^+e^- \to$ hadrons(γ), $e^+e^- \to \mu^+\mu^-(\gamma)$, $e^+e^- \to \tau^+\tau^-(\gamma)$ and $e^+e^- \to e^+e^-(\gamma)$. For Bhabha scattering the selection efficiencies are given for $44° < \theta < 136°$. The efficiencies and background fractions at 170 GeV are the same as the ones quoted for 172 GeV.

		total			high energy		
$e^+e^- \to$ hadrons(γ)							
$\sqrt{s}$ [GeV]	$\mathcal{L}$ [pb^{-1}]	N_{sel}	σ_{had} [pb]	σ_{SM} [pb]	N_{sel}	σ_{had} [pb]	σ_{SM} [pb]
161.3	10.0	1542	155.0 ± 4.2	147.2	423	37.3 ± 2.2	34.9
170.3	1.0	122	123 ± 12	126.6	39	39.5 ± 7.5	29.8
172.3	8.5	1064	123.2 ± 4.2	122.7	248	28.2 ± 2.2	28.9
Systematic Error			1.1%			2.0%	
$e^+e^- \to \mu^+\mu^-(\gamma)$							
$\sqrt{s}$ [GeV]	$\mathcal{L}$ [pb^{-1}]	N_{sel}	$\sigma_{\mu^+\mu^-}$ [pb]	σ_{SM} [pb]	N_{sel}	$\sigma_{\mu^+\mu^-}$ [pb]	σ_{SM} [pb]
161.3	10.9	94	13.4 ± 1.5	11.1	41	4.59 ± 0.84	4.4
172.1	10.2	67	9.9 ± 1.4	9.5	32	3.60 ± 0.75	3.8
Systematic Error			4%			4%	
$e^+e^- \to \tau^+\tau^-(\gamma)$							
$\sqrt{s}$ [GeV]	$\mathcal{L}$ [pb^{-1}]	N_{sel}	$\sigma_{\tau^+\tau^-}$ [pb]	σ_{SM} [pb]	N_{sel}	$\sigma_{\tau^+\tau^-}$ [pb]	σ_{SM} [pb]
161.3	9.8	45	11.2 ± 2.1	11.1	25	4.6 ± 1.1	4.5
172.1	9.7	45	11.8 ± 2.2	9.5	23	4.3 ± 1.1	3.9
Systematic Error			7%			7%	
$e^+e^- \to e^+e^-(\gamma)$							
$\sqrt{s}$ [GeV]	$\mathcal{L}$ [pb^{-1}]	N_{sel}	$\sigma_{e^+e^-}$ [pb]	σ_{SM} [pb]	N_{sel}	$\sigma_{e^+e^-}$ [pb]	σ_{SM} [pb]
161.3	10.2	337	34.0 ± 1.9	35.2	289	30.5 ± 1.8	28.4
170.3	1.0	24	26.1 ± 5.4	31.3	21	24.1 ± 5.3	25.4
172.3	8.8	256	30.8 ± 1.9	30.3	207	26.2 ± 1.8	24.8
Systematic Error			3%			3%	

Table 2: Number of selected events, N_{sel}, measured cross sections, σ, statistical errors and systematic errors and the Standard Model predictions, σ_{SM}, of the reactions $e^+e^- \to$ hadrons(γ), $e^+e^- \to \mu^+\mu^-(\gamma)$, $e^+e^- \to \tau^+\tau^-(\gamma)$ and $e^+e^- \to e^+e^-(\gamma)$, for the total $\sqrt{s'} > 0.1\sqrt{s}$, and the high energy, $\sqrt{s'} > 0.85\sqrt{s}$, event samples. The systematic errors do not include the uncertainty of the luminosity measurement. The cross sections are quoted for the full solid angle except for the Bhabha scattering, given for $44^\circ < \theta < 136^\circ$.

	total				high energy			
$\mathbf{e^+e^- \to \mu^+\mu^-(\gamma)}$								
$\sqrt{s}$ [GeV]	N_f	N_b	A_fb	$A_\mathrm{fb}^\mathrm{SM}$	N_f	N_b	A_fb	$A_\mathrm{fb}^\mathrm{SM}$
161.3	35	21	$0.29^{+0.12}_{-0.14}$	0.29	22	8	$0.59^{+0.13}_{-0.17}$	0.63
172.1	23	16	$0.16^{+0.16}_{-0.17}$	0.29	15	9	$0.31^{+0.18}_{-0.21}$	0.61
Systematic Error	0.05				0.05			
$\mathbf{e^+e^- \to \tau^+\tau^-(\gamma)}$								
$\sqrt{s}$ [GeV]	N_f	N_b	A_fb	$A_\mathrm{fb}^\mathrm{SM}$	N_f	N_b	A_fb	$A_\mathrm{fb}^\mathrm{SM}$
161.3	15	12	$0.16^{+0.19}_{-0.20}$	0.29	12	4	$0.97^{+0.03}_{-0.23}$	0.63
172.1	16	16	$0.07^{+0.18}_{-0.19}$	0.29	9	7	$0.18^{+0.25}_{-0.27}$	0.61
Systematic Error	0.10				0.10			
$\mathbf{e^+e^- \to e^+e^-(\gamma)}$								
$\sqrt{s}$ [GeV]	N_f	N_b	A_fb	$A_\mathrm{fb}^\mathrm{SM}$	N_f	N_b	A_fb	$A_\mathrm{fb}^\mathrm{SM}$
161.3	240	43	0.767 ± 0.049	0.753	206	29	0.819 ± 0.046	0.815
172.1	203	51	0.691 ± 0.058	0.769	176	31	0.796 ± 0.056	0.816
Systematic Error	0.012				0.012			

Table 3: Number of forward, N_f, and backward events, N_b, forward–backward asymmetries, A_fb, statistical errors and systematic errors and the Standard Model predictions, $A_\mathrm{fb}^\mathrm{SM}$, of the reactions $\mathrm{e^+e^-} \to \mu^+\mu^-(\gamma)$, $\mathrm{e^+e^-} \to \tau^+\tau^-(\gamma)$ and $\mathrm{e^+e^-} \to \mathrm{e^+e^-}(\gamma)$ for the total, $\sqrt{s'} > 0.1\sqrt{s}$, and the high energy, $\sqrt{s'} > 0.85\sqrt{s}$, event samples. For the electron pair production both leptons have to be inside $44^\circ < \theta < 136^\circ$.

Parameter	Treatment of Charged Leptons		Standard
	Non–Universality	Universality	Model
$m_{\rm Z}$ [MeV]	91193 ± 10	91193 ± 10	—
$\Gamma_{\rm Z}$ [MeV]	2494 ± 10	2494 ± 10	2497
$r_{\rm had}^{\rm tot}$	2.956 ± 0.029	2.955 ± 0.028	2.967
$r_{\rm e}^{\rm tot}$	0.1410 ± 0.0018	—	
$r_{\mu}^{\rm tot}$	0.1404 ± 0.0017	—	
$r_{\tau}^{\rm tot}$	0.1421 ± 0.0019	—	
$r_{\ell}^{\rm tot}$	—	0.1411 ± 0.0015	0.1426
$j_{\rm had}^{\rm tot}$	0.38 ± 0.29	0.39 ± 0.29	0.22
$j_{\rm e}^{\rm tot}$	-0.07 ± 0.11	—	
$j_{\mu}^{\rm tot}$	0.001 ± 0.064	—	
$j_{\tau}^{\rm tot}$	0.040 ± 0.076	—	
$j_{\ell}^{\rm tot}$	—	0.002 ± 0.045	0.004
$r_{\rm e}^{\rm fb}$	0.0016 ± 0.0018	—	
$r_{\mu}^{\rm fb}$	0.0030 ± 0.0012	—	
$r_{\tau}^{\rm fb}$	0.0046 ± 0.0017	—	
$r_{\ell}^{\rm fb}$	—	0.00307 ± 0.00085	0.00267
$j_{\rm e}^{\rm fb}$	0.65 ± 0.19	—	
$j_{\mu}^{\rm fb}$	0.736 ± 0.089	—	
$j_{\tau}^{\rm fb}$	0.68 ± 0.12	—	
$j_{\ell}^{\rm fb}$	—	0.706 ± 0.066	0.799
χ^2 / DoF	100/127	103/135	—

Table 4: Results of the fits in the S–Matrix framework with and without the assumption of lepton universality.

	$m_{\rm Z}$	$\Gamma_{\rm Z}$	$r_{\rm had}^{\rm tot}$	$r_{\ell}^{\rm tot}$	$j_{\rm had}^{\rm tot}$	$j_{\ell}^{\rm tot}$	$r_{\ell}^{\rm fb}$	$j_{\ell}^{\rm fb}$
$m_{\rm Z}$	1.00	0.05	0.03	0.03	–0.43	–0.19	0.14	–0.04
$\Gamma_{\rm Z}$		1.00	0.80	0.72	–0.01	–0.01	0.04	0.04
$r_{\rm had}^{\rm tot}$			1.00	0.88	0.02	–0.01	0.06	0.05
$r_{\ell}^{\rm tot}$				1.00	0.01	0.05	0.07	0.07
$j_{\rm had}^{\rm tot}$					1.00	0.16	–0.06	0.04
$j_{\ell}^{\rm tot}$						1.00	0.01	0.23
$r_{\ell}^{\rm fb}$							1.00	0.14
$j_{\ell}^{\rm fb}$								1.00

Table 5: The correlation matrix for the 8 parameter S–Matrix fit in Table 4.

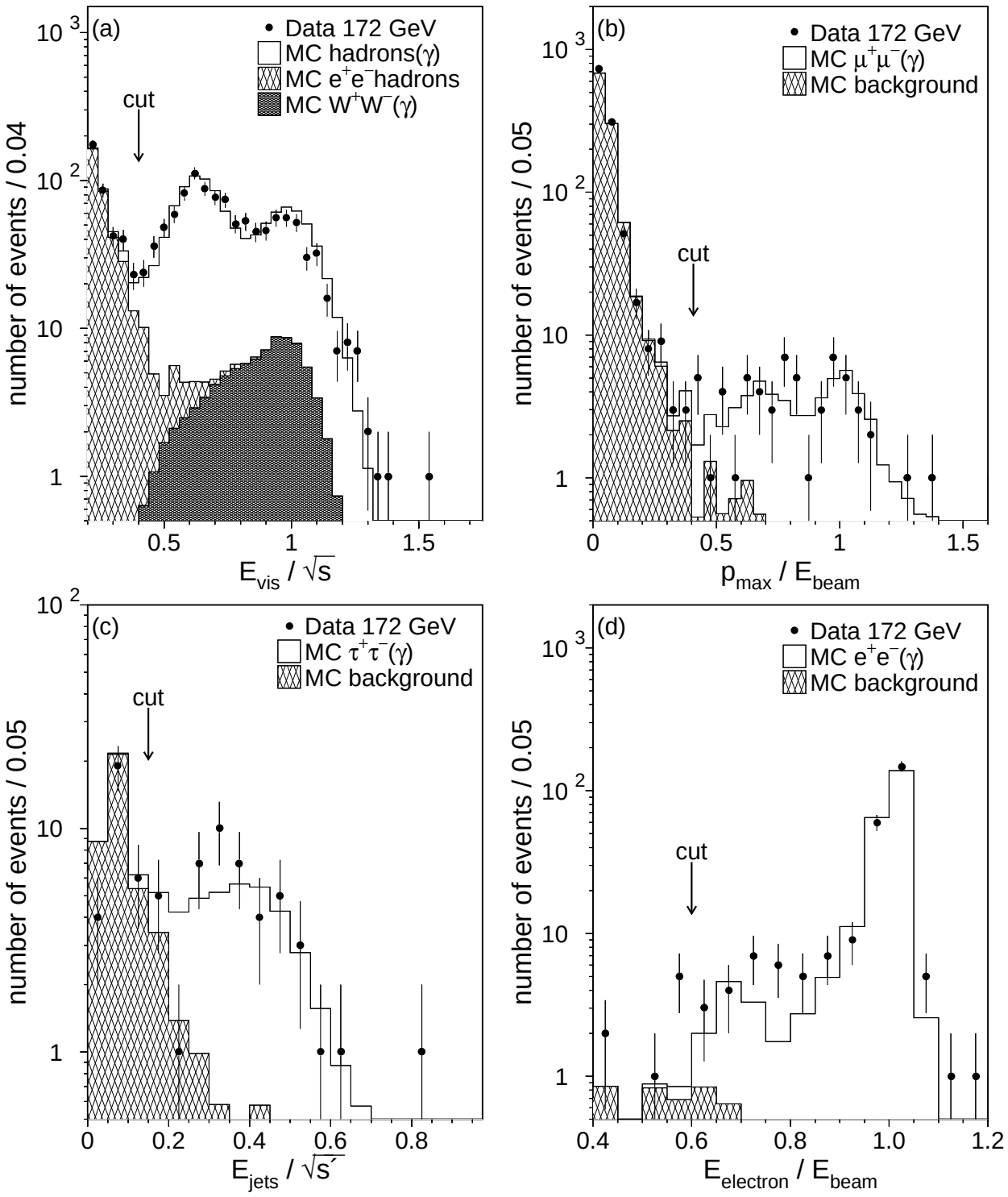

Figure 1: (a) The total visible energy normalised to the centre–of–mass energy, $\sqrt{s}$, for the selection of $e^+e^- \to$ hadrons(γ) events, (b) highest muon momentum for the selection of $e^+e^- \to \mu^+\mu^-(\gamma)$ events, (c) $E_{\rm jets}/\sqrt{s'}$ calculated from the energy of the two tau jets for the selection of $e^+e^- \to \tau^+\tau^-(\gamma)$ events and (d) energy of highest energy electron normalised to the beam energy for the selection of $e^+e^- \to e^+e^-(\gamma)$ events.

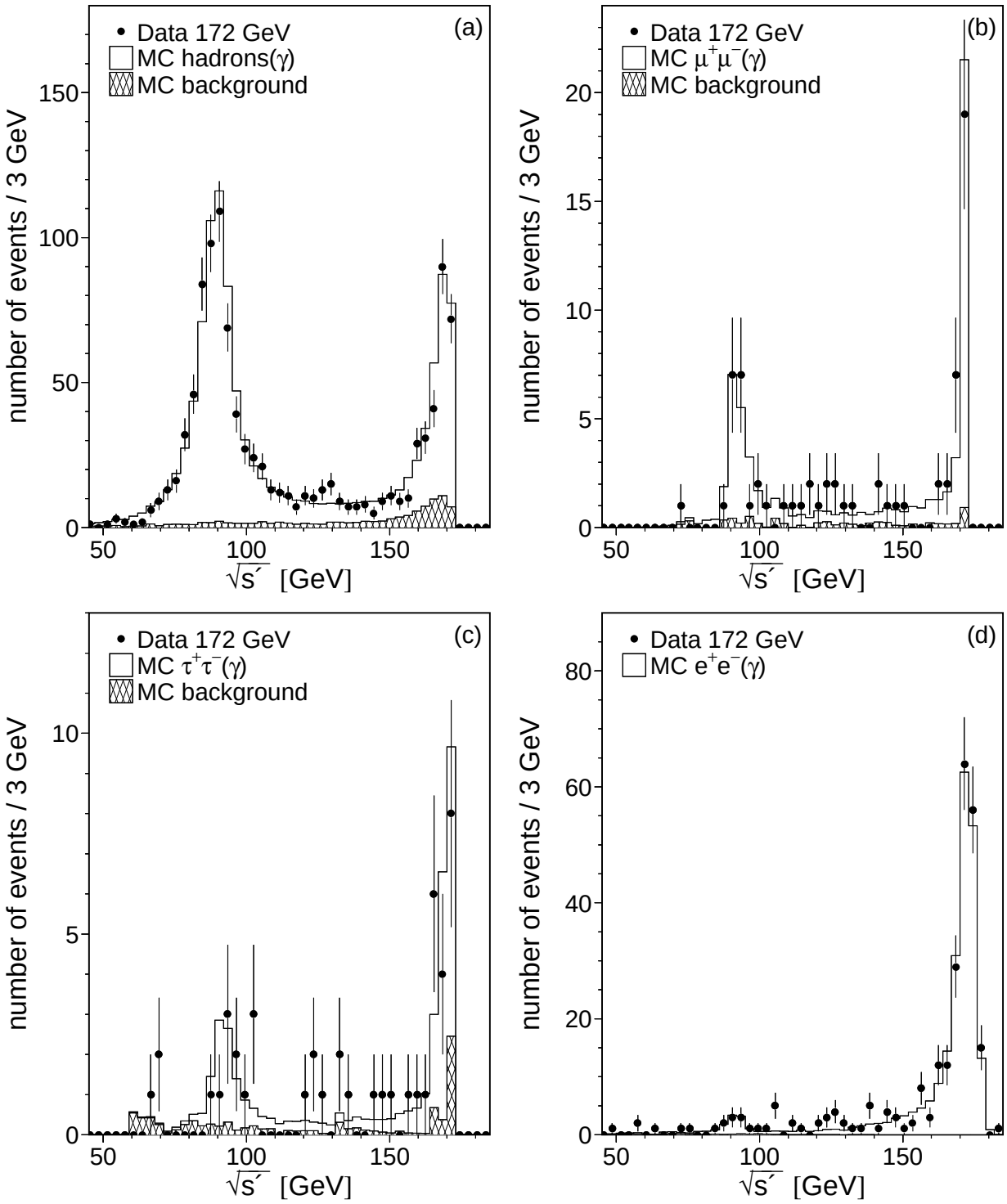

Figure 2: The reconstructed effective centre–of–mass energy, $\sqrt{s'}$, for the selection of (a) $e^+e^- \to$ hadrons(γ) events, (b) $e^+e^- \to \mu^+\mu^-(\gamma)$ events, (c) $e^+e^- \to \tau^+\tau^-(\gamma)$ events and (d) $e^+e^- \to e^+e^-(\gamma)$ events.

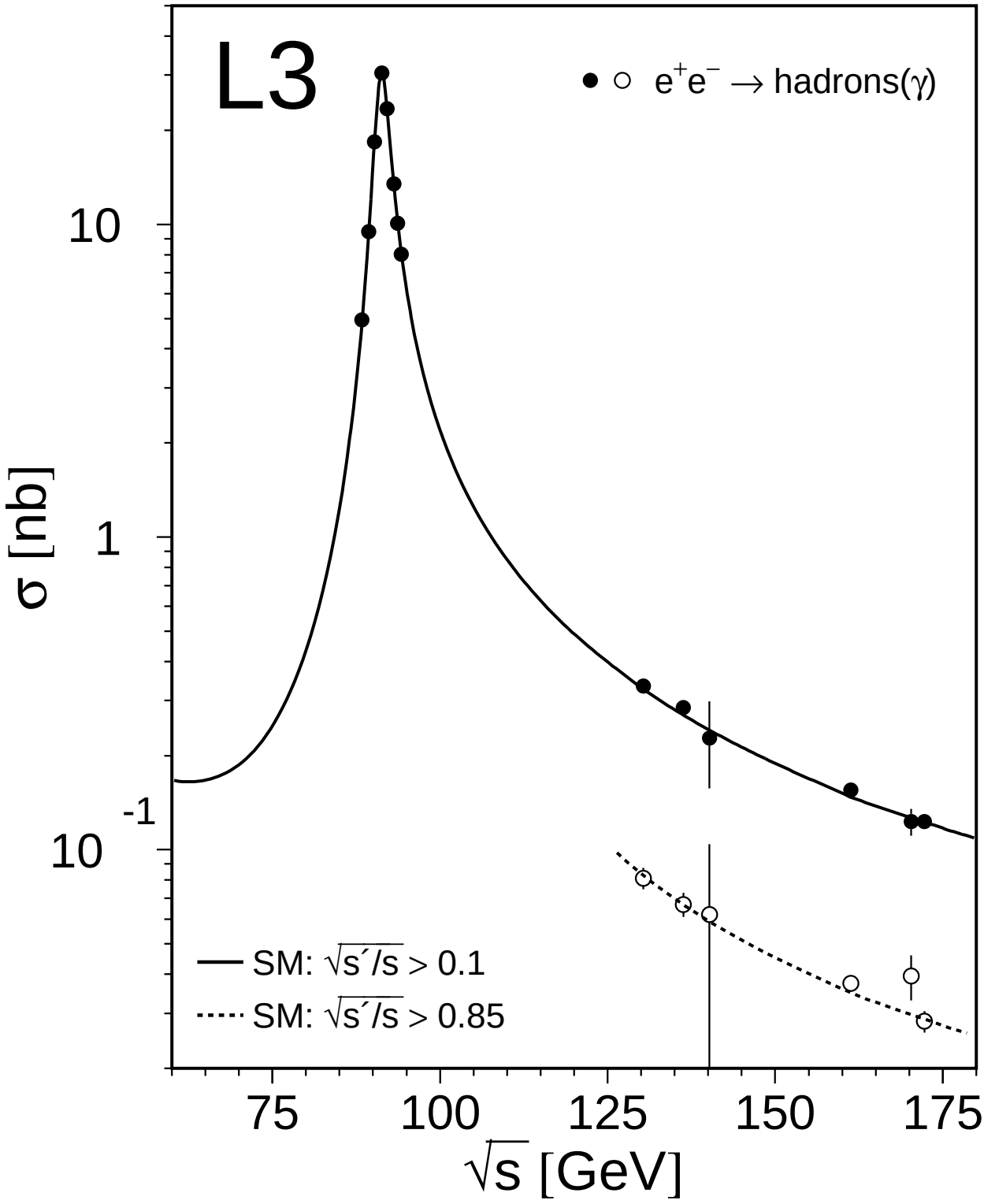

Figure 3: Cross sections of the process $e^+e^- \to$ hadrons(γ), total (solid dots) and the high energy sample (open dots). The Standard Model predictions are shown as a solid line for the total sample and as a dashed line for the high energy sample. The measurements at centre–of–mass energies below 161 GeV have been corrected to correspond to $\sqrt{s'} > 0.1\sqrt{s}$ for the total and $\sqrt{s'} > 0.85\sqrt{s}$ for the high energy event samples. Measurements at the Z peak which are close in centre–of–mass energies have been combined.

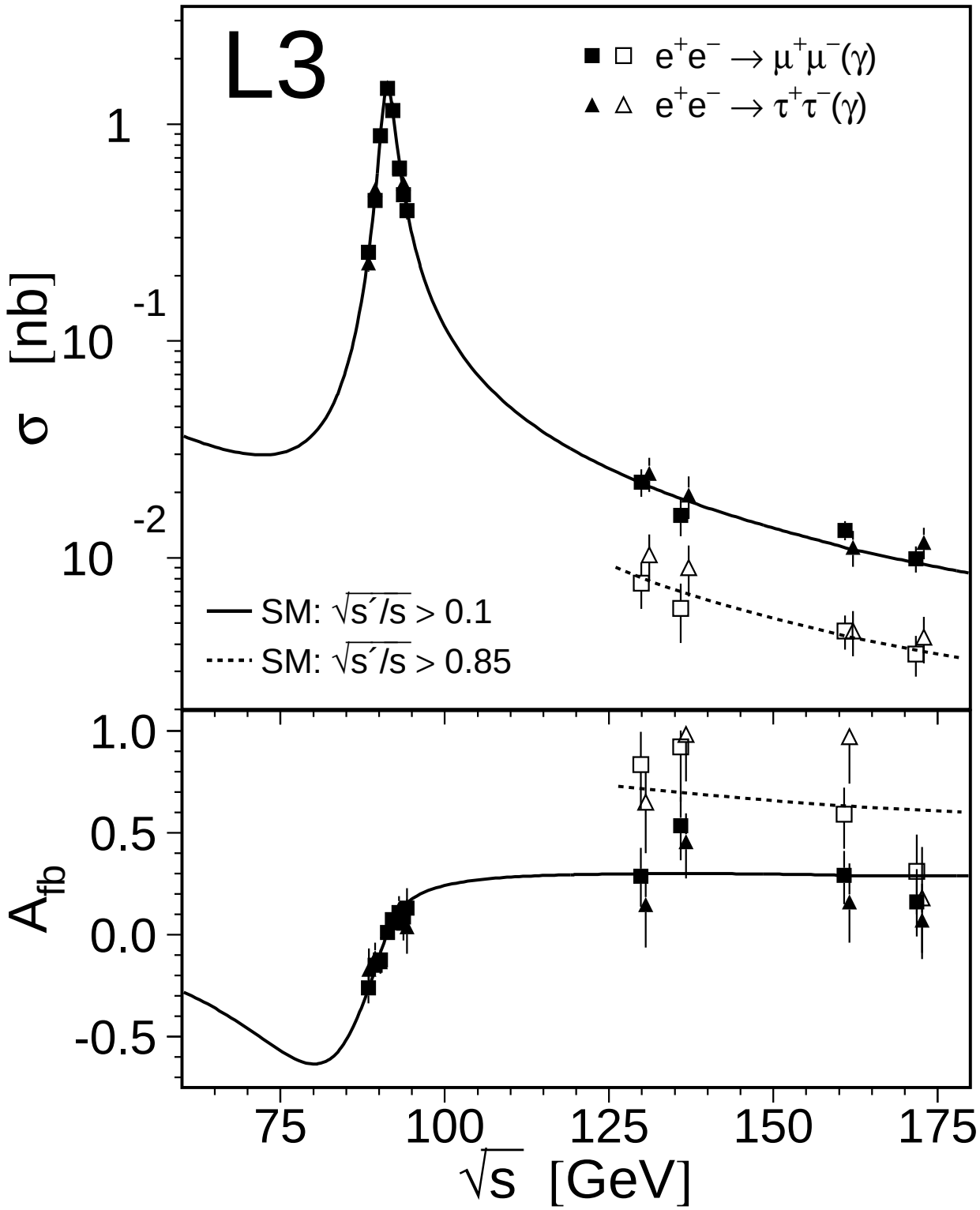

Figure 4: Cross sections and forward–backward asymmetries of the processes $e^+e^- \to \mu^+\mu^-(\gamma)$ and $e^+e^- \to \tau^+\tau^-(\gamma)$ for the total (solid symbols) and the high energy sample (open symbols). The Standard Model predictions are shown as a solid line for the total sample and as a dashed line for the high energy sample. The measurements at centre–of–mass energies below 161 GeV have been corrected to correspond to $\sqrt{s'} > 0.1\sqrt{s}$ for the total and $\sqrt{s'} > 0.85\sqrt{s}$ for the high energy event samples. Measurements at the Z peak which are close in centre–of–mass energies have been combined.

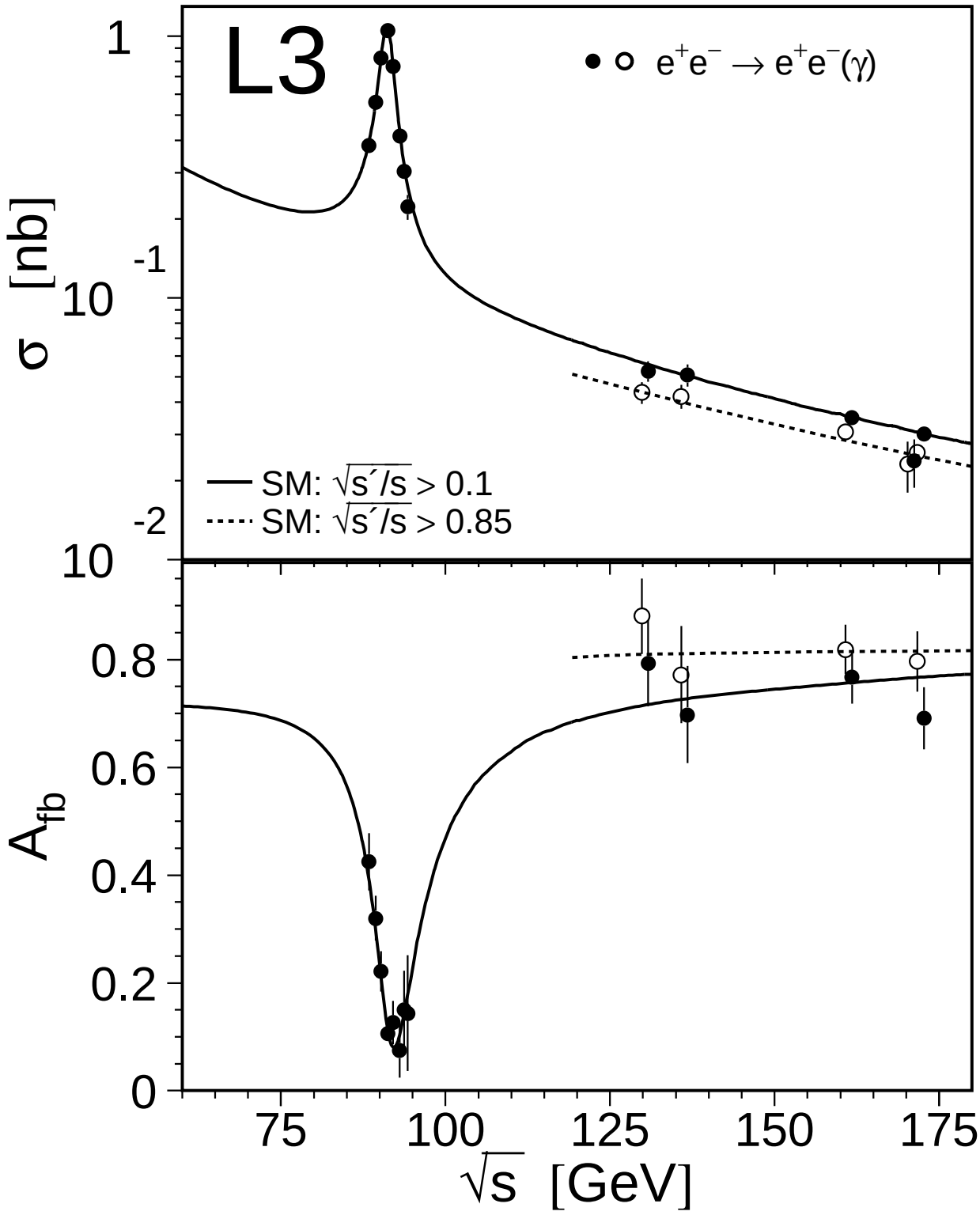

Figure 5: Cross sections and forward–backward asymmetries of the process $e^+e^- \to e^+e^-(\gamma)$ for the total (solid symbols) and the high energy sample (open symbols). The Standard Model predictions are shown as a solid line for the total sample and as a dashed line for the high energy sample. The two electrons are required to be inside $44^\circ < \theta < 136^\circ$. The measurements at centre–of–mass energies below 161 GeV have been corrected to correspond to $\sqrt{s'} > 0.1\sqrt{s}$ for the total and $\sqrt{s'} > 0.85\sqrt{s}$ for the high energy event samples. Measurements at the Z peak which are close in centre–of–mass energies have been combined.

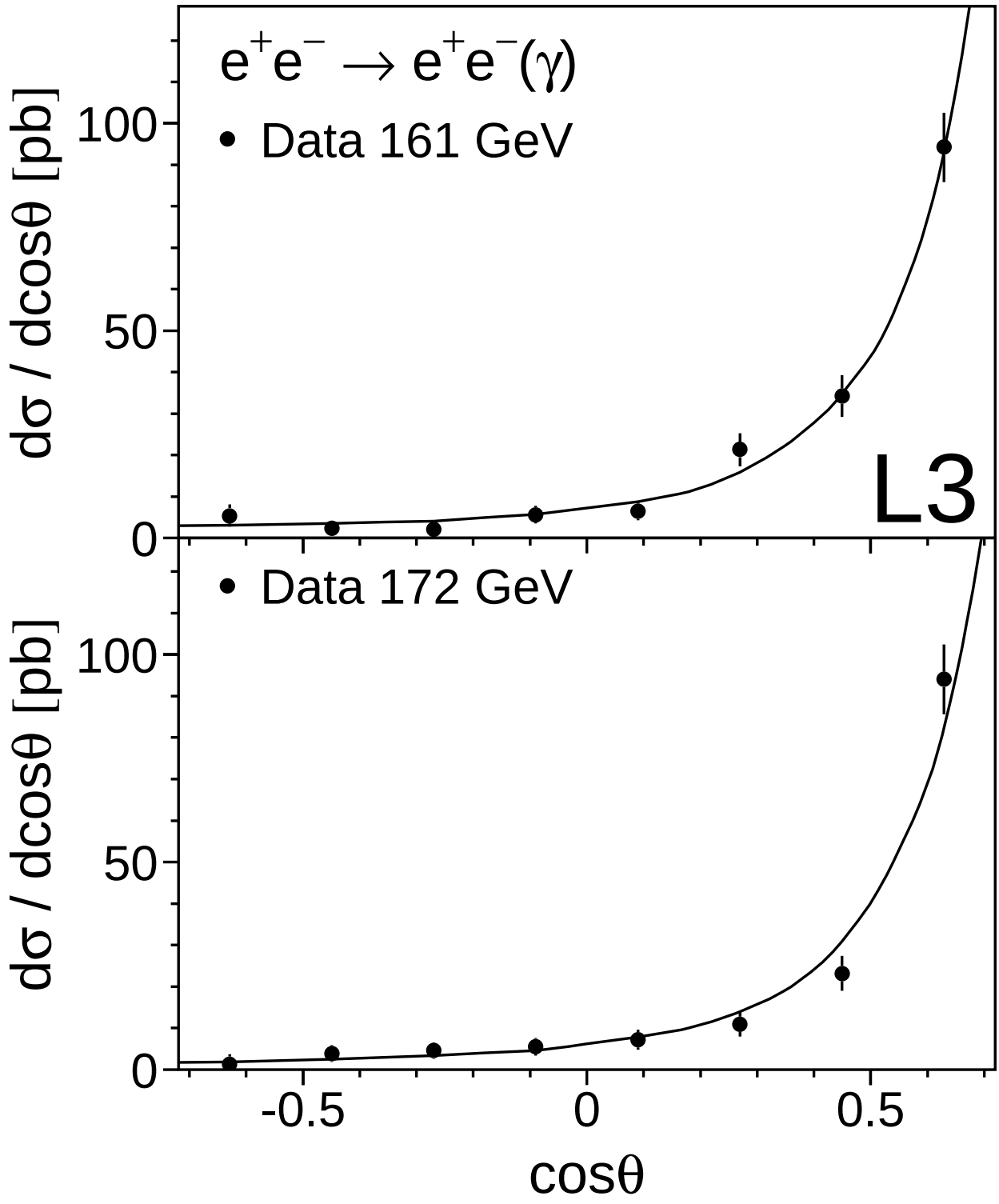

Figure 6: Differential cross section of the high energy event sample, for the process $e^+e^- \to e^+e^-(\gamma)$ at centre–of–mass energies of 161 GeV and 172 GeV. The lines indicate the fit results from which the s–channel asymmetry is obtained.

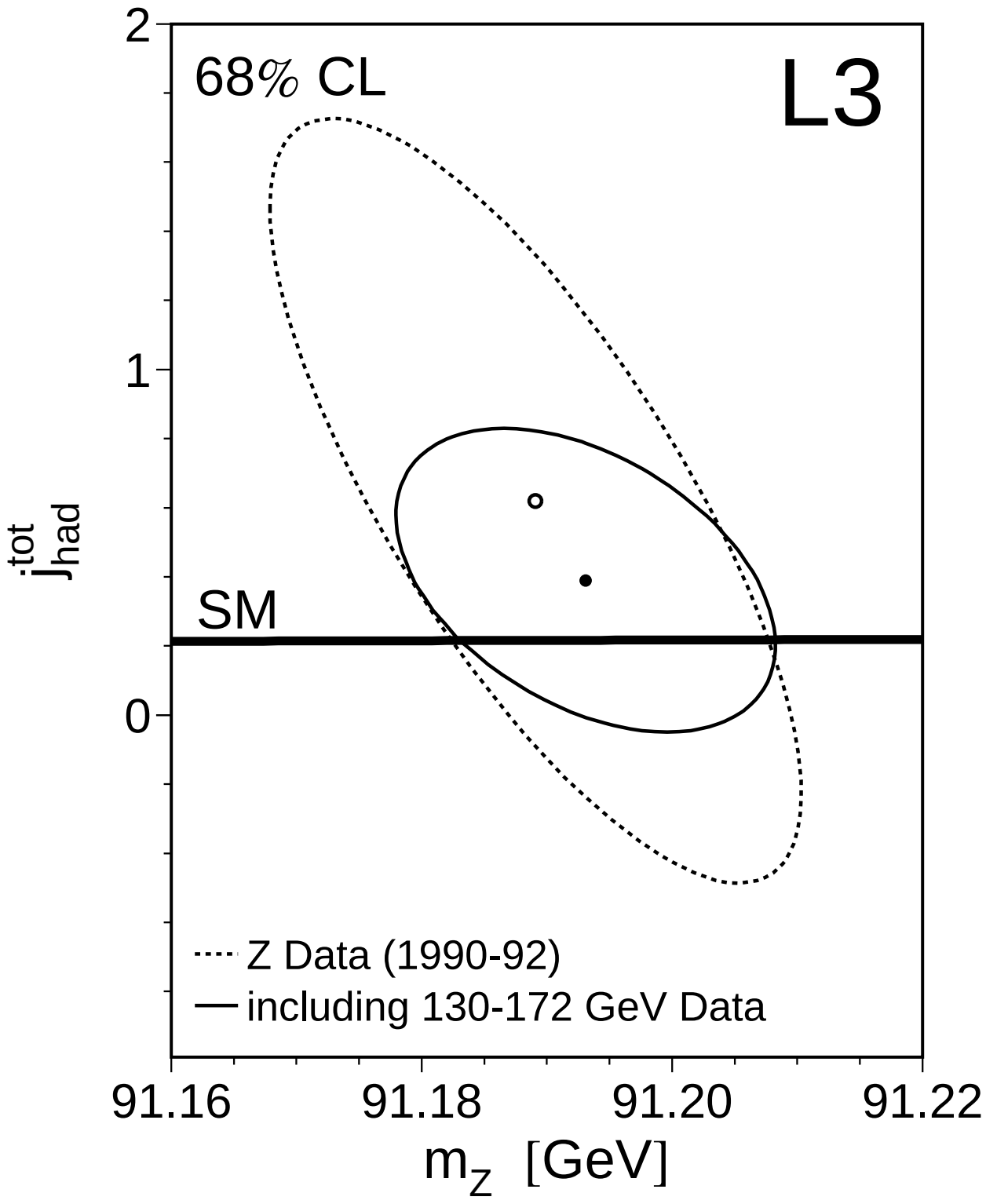

Figure 7: Contours in the (m_{Z}, $\mathrm{j}^{\mathrm{tot}}_{\mathrm{had}}$) plane at 68% confidence level under the assumption of lepton universality. The dashed line shows the Z data only; including the results from 130 GeV to 172 GeV the solid line is obtained. The Standard Model prediction for $\mathrm{j}^{\mathrm{tot}}_{\mathrm{had}}$ is shown as the horizontal band.